

## A case study of damage detection in four-bays steel structures using the HHT approach

Wen-Ko Hsu<sup>1</sup>, Dung-Jiang Chiou<sup>1</sup>, Cheng-Wu Chen<sup>\*2,5</sup>, Ming-Yi Liu<sup>3</sup>,  
Wei-Ling Chiang<sup>4</sup> and Pei-Chiung Huang<sup>4</sup>

<sup>1</sup>Research Center for Hazard Mitigation and Prevention, National Central University, Chung-li, Taoyuan County, Taiwan, R.O.C.

<sup>2</sup>Department of Maritime Information and Technology, National Kaohsiung Marine University, Kaohsiung 80543, Taiwan, R.O.C.

<sup>3</sup>Department of Civil Engineering, Chung Yuan University, Chung-li, Taoyuan County, Taiwan, R.O.C.

<sup>4</sup>Department of Civil Engineering, National Central University, Chung-li, Taoyuan County, Taiwan, R.O.C.

<sup>5</sup>Faculty of Engineering, King Abdulaziz University, Jeddah 21589, Saudi Arabia

(Received April 14, 2013, Revised October 15, 2013, Accepted October 20, 2013)

**Abstract.** This study aims to investigate the relationship between structural damage and sensitivity indices using the Hilbert-Huang transform (HHT) method. Two damage detection indices are proposed: the ratio of bandwidth (RB), and the ratio of effective stiffness (RES). The nonlinear four bays multiple degree of freedom models with various predominant frequencies are constructed using the SAP2000 program. Adjusted PGA earthquake data (Japan 311, Chi-Chi 921) are used as the excitations. Next, the damage detection indices obtained using the HHT and the fast Fourier transform (FFT) methods are evaluated based on the acceleration responses of the structures to earthquakes. Simulation results indicate that, the column of the 1st floor is the first yielding position and the RB value is changed when the RES < 90% in all cases. Moreover, the RB value of the 1st floor changes more sensitive than those from the top floor. In addition, when the structural response is nonlinear (i.e., RES < 100%), the RB and the RES curves indicate the incremental change in the HHT spectra. However, the same phenomenon can be found from FFT spectra only when the stiffness reduction is large enough. Therefore, the RB estimated from the smoothed HHT spectra is an effective and sensitive index for detecting structural damage.

**Keywords:** HHT; damage detection index; effective stiffness; sensitivity

### 1. Introduction

Natural disaster, like the typhoon, flood, tsunami, drought and earthquake, causes the serious damage to people and commercial frequently. Some references of Damage assessment and uncertainty analysis were published to mitigate the threaten of casualty (Shiau *et al.* 2006, Maung *et al.* 2009, Kao and Govindaraju 2010 and Hsu *et al.* 2011, 2012). In addition, Structural health monitoring (SHM) has received considerable attention recently in structural engineering. While SHM attempts to detect structural damage in buildings, various approaches have been developed

---

\*Corresponding author, Dr., E-mail: [chengwu@mail.nkmu.edu.tw](mailto:chengwu@mail.nkmu.edu.tw)

for detecting damage based on various methods (Sun *et al.* 2002, Lei *et al.* 2003, Sohn *et al.* 2003, Kim and Melhem 2004, Yu and Giurgiutiu 2005, Rucka *et al.* 2006, Lanata and Del Grosso 2006, Zhanga *et al.* 2007, Wang *et al.* 2007, Ren *et al.* 2008, Bindhu *et al.* 2008, Hakan *et al.* 2009, Zhang and Xu 2009, Nair *et al.* 2009 and Akanshu *et al.* 2010, Kuok and Yuen 2012).

Several previous studies have proposed that the empirical mode decomposition (EMD) and Hilbert–Huang transform (HHT) methods can be used for nonstationary and nonlinear time series analysis (Huang *et al.* 1998, 1999). These methods have also been extensively adopted for the detection of structural damage. Based on EMD and HHT, Yang *et al.* (2000a) proposed the notion of identifying MDOF linear structural systems using the measured impulse response time history. The intrinsic mode functions (IMFs) decomposed by EMD are shown to be the modal responses. The Hilbert transform is then applied to each IMF in order to obtain the amplitude and phase angle so as to identify the physical mass, stiffness and proportional damping matrices of the structures. Later, Yang *et al.* (2000b) indicated that an IMF may involve the contribution of a complex conjugate pair of modes with a unique frequency and a damping ratio, referred to as the modal response. Additionally, all modal responses can be obtained from the IMFs. Each modal response is then decomposed in the frequency-time domain to yield an instantaneous phase angle and amplitude as functions of time when using the Hilbert transform to identify the non-proportional damping of the linear structure.

Zhang *et al.* (2003) indicated that HHT-based Hilbert spectra can clearly reveal the temporal-frequency energy distribution for motion recordings. The normal modes are assumed to exist for MDOF systems. Based on the Hilbert-Huang spectral analysis, Yang *et al.* (2003a) proposed a linear least-square fit procedure to identify the natural frequency and damping ratio from the instantaneous amplitude and phase angle for each modal response. Frequently, all eigenvalues and eigenvectors of linear structures are found to be complex (Yang *et al.* 2003b). The HHT based method has been extended further to identify general linear structures with complex modes using the free vibration response data polluted by noise. Although structural damage information is generally extracted from the measured data, recorded acceleration data in the damage location normally have a discontinuity relationship in a spectrum when the damage event occurs. Huang *et al.* (1998, 1999) showed the feasibility of using EMD and HHT to decompose a signal in the time-frequency domain more precisely than wavelet analysis can. Consequently, two methods were proposed based on EMD and HHT for detecting structural damage (Yang *et al.* 2004). The first method extracts damage spikes due to a sudden change of structural stiffness from the measured data. The damage time instant and damage locations can then be detected. The second method can detect the damage time instant and determine the natural frequencies and damping ratios of the structure before and after damage. These two proposed methods are then applied to a benchmark problem. According to those results, the proposed methods can detect damage and evaluate related structures efficiently.

Besides, the stiffness and damping matrices cannot be identified quantitatively and the stiffness in each story is not assessed before and after the damage occurs. Therefore, the HHT method is further applied to the phase I IASC–ASCE benchmark building to completely identify stiffness and damping coefficients before and after damage (Lin *et al.* 2005). The method consists of three steps: obtaining the cross-correlation functions from simulated ambient vibration data; identifying the modal parameters from the cross-correlation functions; and identifying the structural stiffness and damping from modal parameters. Then, each story unit prior to and after damage is compared in terms of stiffness to identify the damaged locations and severities. The method was also adopted in a previous study (Darryll *et al.* 2006) in order to process the time series data from a variety of

1-D structures with and without structural damage so as to obtain the magnitude, phase and damping information. The location and extent of damage incurred can be determined by tracking the phase properties between successive degrees of freedom. Also, analysis results of the acceleration responses of the damaged structures clearly reveal increases in damping. Based on HHT and a sliding-window fitting (SWF) technique, (Pai *et al.* 2008) proposed a time-frequency signal processing method for parametric and non-parametric identification of nonlinear dynamical systems. The maximum displacement states are used to determine the stiffness and the velocity states to find the velocity-damping curve. The accurate parametric and non-parametric identifications are provided from several nonlinear numerical simulations.

However, the mode mixing problem often occurs with the HHT method when intermittency is involved in the data. A new ensemble empirical mode decomposition (EEMD) method (Wu and Huang 2004) was proposed to overcome the intermittence phenomenon. The latest new HHT ensemble skills method has been utilized to analyze the Tai-power Building's strong-motion station records from 1994-2006 (Su *et al.* 2008). According to those results, the acceleration relations between the basement and the 27th story (top) are not proportional, even when the building maintains elasticity. A HHT-based damage detection method for two moment frames building is proposed (Raufi 2010). The results show the rotational response of nodes to be the best option to detect damage of frames. Alvanitopoulos *et al.* (2010) proposed novel crucial characteristic seismic parameters for the damage indicators of the structures. Two structural damage indices, the maximum amplitude ( $A_{\text{HHT\_max}}$ ) and the mean amplitude ( $A_{\text{HHT\_mean}}$ ), are proposed. A set of 13 natural accelerograms from well-known sites worldwide with strong seismic activity have been used. Results indicate a high correlation between the new seismic parameters ( $A_{\text{HHT\_max}}$ ,  $A_{\text{HHT\_mean}}$ ) and the damage indices.

The relationship between structural damage and the sensitivity indices is obtained using the HHT method (Chiang *et al.* 2011). Three sensitivity indices are proposed: the ratio of rotation (RR), the ratio of shifting value (SV) and the ratio of bandwidth (RB). Simulation results indicate that the RB obtained from the HHT spectra displays a trend of incremental change with an increasing RR, making it an effective and sensitive index for detecting structural damage. Next, a damage index, the ratio of bandwidth (RB) is used to demonstrate the effectiveness from real steel models for detecting structural damage (Chiou *et al.* 2011). Results indicate that, when the response of the structure is in the elastic region, the RB value only slightly changes in both the HHT and the fast Fourier transform (FFT) spectra. Additionally, RB values estimated from the HHT spectra vs. the PGA values change incrementally when the structure response is nonlinear i.e., member yielding occurs, but not in the RB curve from the FFT spectra.

Tang *et al.* (2011) proposed a different damage detection index, the ratio of equivalent damping ratio (RED). It is evaluated using the FFT and HHT methods for analysis of the shaking table test data obtained from the benchmark models. The results show that the RED estimated from the smoothed HHT spectra is an effective and sensitive index for detecting structural damage. Furthermore, the changes in RED present more sensitivity at the top floor than other floors. The proposed RED strategy will be used to establish an on-line health monitoring scheme for detecting structural damage in steel structures right after the occurrence of ground motion. The time-varying instantaneous frequency, instantaneous energy and relative amplitude of Hilbert marginal spectrum are used to identify the damage evolution and location of the structure by Han *et al.* (2011). The shaking table test of a 12-storey reinforced concrete frame model is adapted to demonstrate the proposed approach is capable to identify damage of the structure. Atul *et al.* (2011) propose an improved HHT combined with wavelet packet decomposition for diagnosis of damage in

structures. Numerical simulation studies have been conducted by solving a bridge girder as a numerical example to validate the proposed time series analysis based damage diagnostic method. Results present the combined wavelet packet and EMD based sifting process can successfully decompose a signal into components with simple frequency content. Kunwar *et al.* (2013) generate a single-span bridge instrumented with 10 wireless sensor nodes to obtain the transient vibration data for detecting damage using HHT method. Three levels of damages were introduced by removing bolts connecting the central cross member with one of the girders. Analyzed results indicate that the ability of the HHT method to detect and locate damage clearly even under transient vibration loads.

Referring to the results of Chiang *et al.* (2011) and Tang *et al.* (2011), the single bay MDOF models are constructed to obtain the acceleration spectra based on the HHT and FFT methods during earthquakes. In fact, a multiple bays model can be found easily in a real structure. Whether the damage detection index, RB (or RED) proposed by Chiang *et al.* (2011) keeping provide the sensitivity of damage detection in a complex structure or not, the objective of this study is to discuss the relationship between RB and the change of ratio of effective stiffness, RES for four bays steel structure subjected to earthquakes. First, the three, five and ten story four bays steel models are established using the SAP2000 program. Two types time history earthquake data (Japan 311, Chi-Chi 921) are adopted as the excitations. Next, the rotational stiffness of columns of these structures is then simulated using Wen's model (Wen 1976). The nonlinear time history analysis is used to generate the acceleration data from models. Then the damage indices, RB and RES can be obtained from HHT and FFT spectra separately based on the acceleration responses of the structures to earthquakes. Additionally, Tang *et al.* (2011) shows the trend of RB in top floor is more sensitive than other floors while the nonlinearity is happened to a structure. In this study, the change of RB in the first yielding floor will be discussed with the top floor deeply to demonstrate the RB of roof provides more sensitivity than other floors.

## 2. Hilbert -Huang Transformation (HHT)

The HHT, developed by Huang *et al.* (1998, 1999), consists of a two step-empirical mode decomposition (EMD) and the Hilbert spectral analysis (HSA). The principles and procedures for the HHT method are briefly summarized in this section. Detailed information can be found in the quoted references (Huang *et al.* 1998, 1999).

### (1) Empirical Mode Decomposition (EMD):

The EMD method involves the extraction of the IMFs from a given time series. An IMF is a function that satisfies two conditions as follows:

(a) In a whole data set, the number of extrema and the number of zero crossings must either be equal or differ at most by one.

(b) At any point, the mean value of the envelope defined by the local maxima and the envelope defined by the local minima is zero.

Once all IMFs are sifted from a given signal  $x(t)$ , it can be expressed as follows

$$x(t) = \sum_{i=1}^n c_i(t) + r_n(t) \quad (1)$$

where  $n$  is the total number of the IMFs, and  $r_n(t)$  denotes the final residue which represents the DC component (constant term) containing the overall trend of  $x(t)$ . The  $c_i(t)$  are almost orthogonal to each other and have nearly zero means.

Hilbert Spectral Analysis:

For an arbitrary time series  $X(t)$ , the Hilbert transformation,  $Y(t)$ , is defined as follows

$$Y(t) = \frac{1}{\pi} P \int_{-\infty}^{\infty} \frac{X(t')}{t-t'} dt' \tag{2}$$

where  $P$  indicates the Cauchy principal value.

With this definition,  $X(t)$  and  $Y(t)$  can be combined to form the analytical signal  $Z(t)$

$$Z(t) = X(t) + iY(t) = a(t)e^{i\theta(t)} \tag{3}$$

where

$$a(t) = [X^2(t) + Y^2(t)]^{1/2}, \quad \theta(t) = \arctan\left(\frac{Y(t)}{X(t)}\right)$$

From the polar coordinate expression in Eq. (3), the instantaneous frequency can be defined as

$$\omega(t) = \frac{d\theta(t)}{dt} \tag{4}$$

Applying the Hilbert transform to the IMFs components of  $X(t)$  in Eq. (3), the data  $X(t)$  can be written as follows

$$X(t) = \Re \sum_{j=1}^n a_j(t) e^{i \int \omega_j(t) dt} \tag{5}$$

where  $\Re$  is the real part of the value.

Similar to the Fourier amplitude spectrum, the Hilbert amplitude spectrum  $H(\omega, t)$  is the time-frequency distribution of the amplitude. The marginal spectrum  $h(\omega)$  is a measure of the total amplitude (or energy) contribution from each frequency value. It represents the accumulated amplitude over the entire data span in a probabilistic sense. The marginal spectrum is obtained by the integration of the Hilbert spectrum over the time duration  $T$

$$h(\omega) = \int_0^T H(\omega, t) dt \tag{6}$$

### 3. Sensitivity of damage detection

#### 3.1 Damage detection index

Structural damage is usually represented by the natural frequency and the damping ratio of the structure changes when any structural member is damaged due to strong ground motion. The most obvious of these indexes is the change in the equivalent damping ratio of the structure before and after damage by earthquakes. Furthermore, a damage detection index, the ratio of an equivalent damping ratio RED, has been derived by Tang *et al.* (2011). The procedures of the derivation are briefly summarized as follows:

As is well known, the half-power bandwidth (Chopra 2001) is related to the equivalent damping ratio of an SDOF structure. Then the definition of the ratio of bandwidth RB can be expressed as follows

$$RB = \frac{f'2 - f'1}{f2 - f1} \quad (7)$$

where the bandwidth  $(f2 - f1)$  or  $(f'2 - f'1)$  denotes the half-power bandwidth, as estimated from the acceleration frequency response curve Ra, as shown in Fig. 1.

Next, the relationship of the half-power bandwidth  $(f2 - f1)$  vs. damping ratio  $\zeta_0$  of the structure can be expressed as follows

$$\zeta_0 = \frac{f2 - f1}{2f_0} = \frac{f2 - f1}{f2 + f1} \quad (8)$$

where  $f_0$  represents the natural frequency of the structure.

Similarly, the equivalent damping ratio  $\zeta_{eq}$  estimated from another spectrum, as computed from the structural responses to a stronger ground motion, can be expressed as follows

$$\zeta_{eq} = \frac{f'2 - f'1}{2f_{eq}} = \frac{f'2 - f'1}{f'2 + f'1} \quad (9)$$

where  $f_{eq}$  represents the equivalent natural frequency of the structure.

By using Eqs. (8) and (9), the ratio of equivalent damping ratio RED can be expressed as follows

$$RED = \frac{\zeta_{eq}}{\zeta_0} = \frac{f'2 - f'1}{f2 - f1} \times \frac{f_0}{f_{eq}} = RB \times \frac{f_0}{f_{eq}} \quad (10)$$

Since  $f_0/f_{eq} \geq 1$  and normally is approximately close to 1 except for a situation in which the attack ground motion is very strong, it is assumed that the value of  $f_0/f_{eq} \cong 1$ . Therefore, the ratio of bandwidth RB is highly correlated with or approximately equal to the ratio of equivalent damping ratio, and can be used as an index for damage detection. Notably, since the half-power bandwidth is difficult to estimate from an original structural response spectrum, the moving average skill (Chou 1975) is used to smooth the spectrum. Index RED (or RB) is then evaluated from the smoothed curves as shown in Fig. 1.

Besides, the change of stiffness to a member can be observed when the structure is in nonlinear

region. Fig. 2 shows the hysteresis of a column during a strong ground motion. The change of stiffness can be expressed to a new damage detection index, the ratio of effective stiffness, RES. The derivation of RES is shown as follow

$$K_{eff} = \min\left(\frac{M_{max}}{R_{max}}, \frac{M_{min}}{R_{min}}\right) \tag{11}$$

$$RES(\%) = \frac{K_{eff}}{K_0} \tag{12}$$

In which, the  $K_{eff}$  can be calculated from a hysteresis taking the minimum positive stiffness or negative stiffness to the structure during an excitation. Then the RES can be evaluated from  $K_{eff}$  to  $K_0$ . Hence, if RES=100%, the structure remains in the elastic region. However, if RES<100%, the nonlinear behavior of the structure exists and is revealed in the acceleration responses.

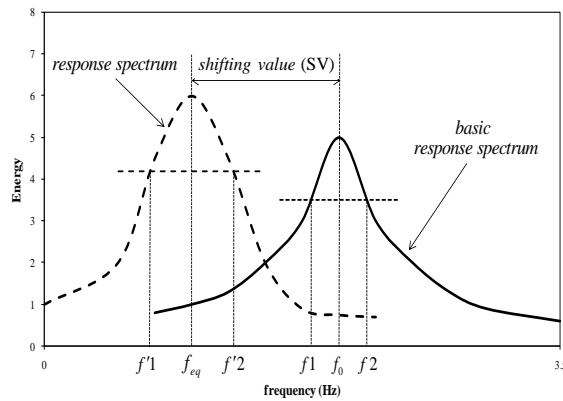


Fig. 1 Definition of the ratio of bandwidth (RB) and definition of the ratio of equivalent damping ratio (RED) (Tang *et al.* 2011)

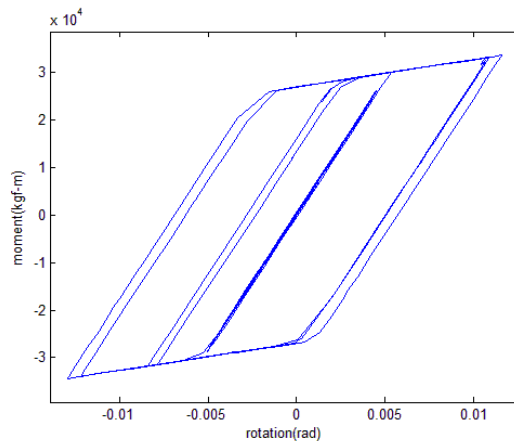


Fig. 2 Definition of the ratio of effective stiffness (RES)

### 3.2 Sensitivity of detecting damage to MDOF models

Fig. 3 presents four bays three, five and ten story steel models generated by the SAP2000 program. The length of one bay is 3 m and the height of one story is 4 m.

Table 1 lists the member section and the modal frequency of these models. The rotational stiffness of columns of these structures is then simulated using Wen's model (Wen 1976). Furthermore, the Japan 311 (MYG010, IWT026, TCG009) and Chi-Chi (TCU138, CHY008, ILA061) earthquakes are adopted as the excitations. The detail information of stations, time history records are shown in Table 2 and Fig. 4.

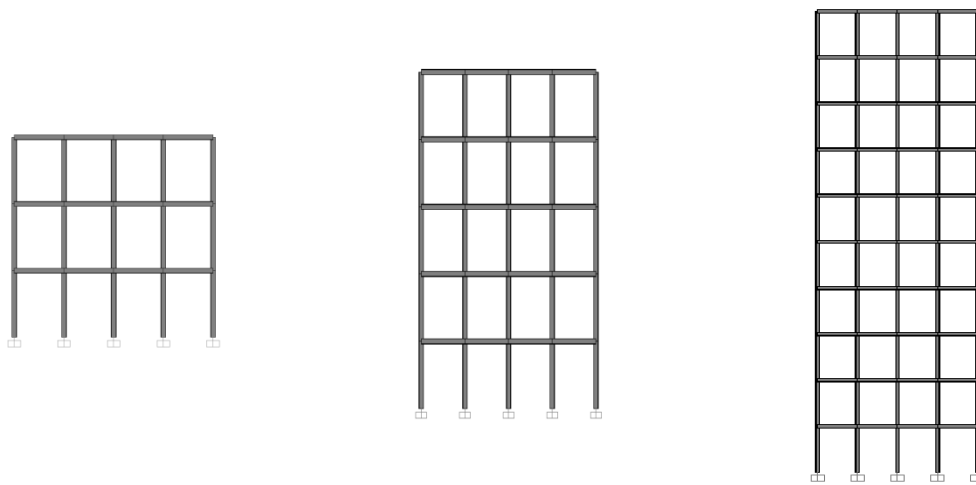


Fig. 3 Four bays MDOF steel structures with three types

Table 1 Modal frequency and frame section of the structures

		Three-story	Five-story	Ten-story
Section	Beam	W12X22	W12X22	W12X22
	Column	W18X35	W18X35	W18X35
Modal frequency (Hz)	$f_1$	3.4	2.0	1.0
	$f_2$	11.2	6.4	3.4
	$f_3$	20.2	12.0	5.8

Table 2 Information of earthquake stations

Name	Station No.	Location	latitude	longitude
Japan 311	MYG010	Miyagi	38.4252	141.2809
	IWT026	Iwate	39.2569	141.0983
	TCG009	Tochigi	36.7258	139.7155
Chi-Chi 921	TCU138	Taichung	24.1832	120.9307
	CHY008	Chaiyi	23.4853	120.2691
	ILA061	Yilan	24.5757	121.8438

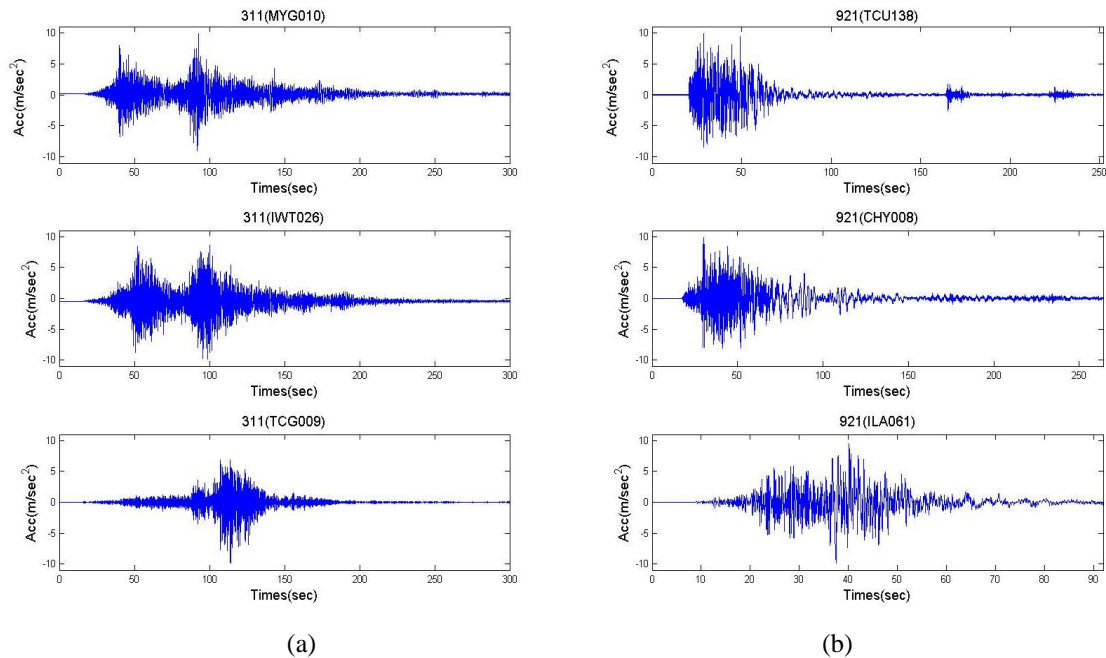


Fig. 4 Time history records of Japan 311 and Chi-Chi 921 earthquakes

Next, the acceleration responses of the floor for each case are evaluated after inputting the adjusted Japan 311 and Chi-Chi 921 earthquake excitations (PGA = 0.1, 0.2, 0.3, 0.4, 0.5, 0.6, 0.8 and 1.0 g). In which, for example, if the first yielding point is occurred at PGA=0.2 g, the increment of PGA value changes to 0.02 g (0.2 g, 0.22 g, 0.24 g, ..., 0.3 g). Then the change of RES and RB can be observed more clearly before and after yielding of the structure. There are 18 response cases (three models and six earthquakes) used to evaluate the damage indices. The sensitivity indices RB and RES are computed from the acceleration response data using the HHT and FFT methods. Given the difficulty in estimating the bandwidth based on the original structural response spectrum, the moving average method with span 3 (Chou 1975) is used to smooth the spectrum to evaluate the indices.

A portion of the above results are summarized in Table 3 and Figs. 5-12. Fig. 5 displays the moment-rotation curve of the first yielding member, which is at the bottom of the first floor column in the three-story model for a predominant frequency of  $\theta_{min}$ ,  $M_{min}$ ,  $\theta_{max}$  and  $M_{max}$ , which are used to evaluate the RES. It should be noted that  $M_y$  and  $\theta_y$  can be observed from the stress-strain curve of the material, as has been used in Wen's model (Wen 1976). For instance, the first yielding of column occurred in the PGA=0.26g case. The RES=98.03% can be evaluated for this case as shown in Table 3. Next, the RES decreases with an increasing PGA value. The RES reduces to 52.37% obtained from the moment-rotation curve in the PGA=1.0g case.

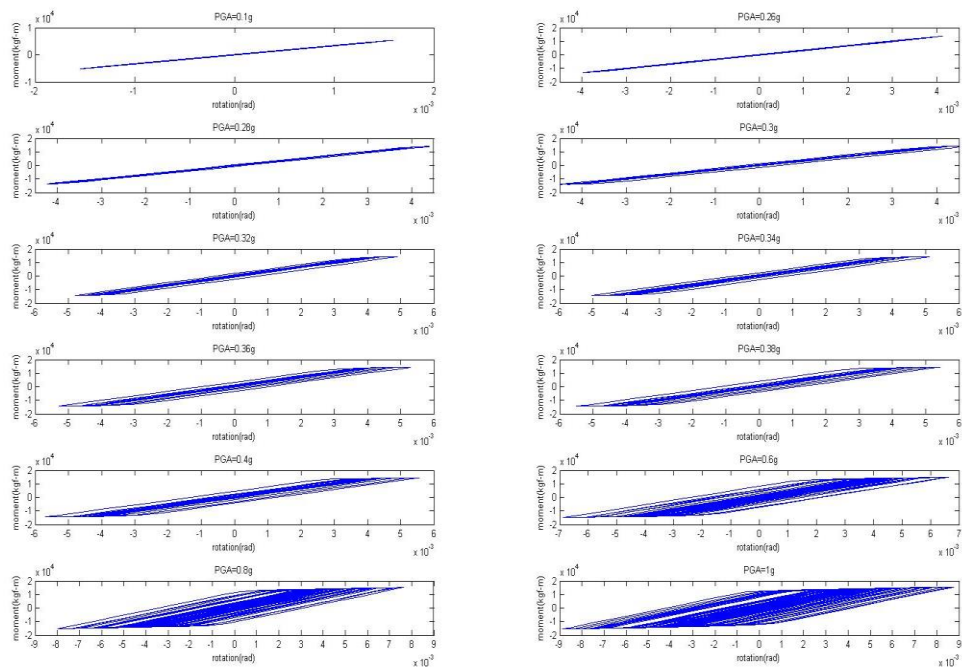


Fig. 5 Hysteresis of the bottom of the first floor column for three-story cases (TCG009)

Table 3 Results of RB vs. RES (three-story, TCG009; ten-story, ILA061)

Three-story 311 (TCG009)												
FFT												
PGA	0.1g	0.26g	0.28g	0.03g	0.32g	0.34g	0.36g	0.38g	0.4g	0.6g	0.8g	1g
RB(1F)	1	1.0006	1.0021	1.0059	1.009	1.0132	1.0181	1.0234	1.0287	0.994	0.9876	1.0072
RB(3F)	1	1.0001	1.0005	1.0016	1.0036	1.0063	1.0112	1.018	1.0272	1.0014	1.0102	0.9848
RES	100.00%	98.03%	94.86%	90.66%	86.70%	83.49%	81.00%	78.39%	76.11%	64.68%	57.10%	52.37%
HHT												
PGA	0.1g	0.26g	0.28g	0.3g	0.32g	0.34g	0.36g	0.38	0.4g	0.6g	0.8g	1g
RB(1F)	1.0000	1.0029	1.0184	1.0624	1.1268	1.1366	1.1400	1.1458	1.1509	1.1569	1.1818	1.1871
RB(3F)	1.0000	1.0016	1.0145	1.0588	1.1211	1.1222	1.1251	1.1299	1.1375	1.1620	1.1971	1.2110
RES	100.00%	98.03%	94.86%	90.66%	86.70%	83.49%	81.00%	78.39%	76.11%	64.68%	57.10%	52.37%
Ten story 921 (ILA061)												
FFT												
PGA	0.1g	0.28g	0.3g	0.32g	0.34g	0.36g	0.38g	0.4g	0.42g	0.6g	0.8g	1g
RB(1F)	1	1.0005	1.0013	1.0025	1.0038	1.005	1.006	1.0064	1.0061	0.9812	0.9837	1.0021
RB(10F)	1	1.0005	1.0014	1.0026	1.004	1.0053	1.0066	1.0076	1.0084	1.0074	0.9898	0.9853
RES	100.00%	95.42%	90.42%	85.27%	80.62%	76.59%	73.07%	69.93%	67.10%	51.12%	41.71%	36.00%
HHT												
PGA	0.1g	0.28g	0.3g	0.32g	0.34g	0.36g	0.38g	0.4g	0.42g	0.6g	0.8g	1g
RB(1F)	1.0000	1.0358	1.0917	1.1769	1.2420	1.2993	1.3677	1.4223	1.4780	1.5712	1.6707	1.7545
RB(10F)	1.0000	1.0301	1.0850	1.1666	1.2353	1.2921	1.3614	1.4269	1.4821	1.5998	1.7096	1.8501
RES	100.00%	95.42%	90.42%	85.27%	80.62%	76.59%	73.07%	69.93%	67.10%	51.12%	41.71%	36.00%

Figs. 6 and 7 present the acceleration response spectra (PGA=0.1g, 0.6g, 0.8g and 1.0g) for three-story models from first and top floor using the FFT and HHT methods respectively. Both the change of bandwidth in the predominant frequency cannot be observed clearly at 1F and 3F from FFT spectra in the 311 (TCG009) cases as shown in Fig. 6. Opposite to the FFT spectra, the change of bandwidth can be seen obviously when the responses of three-story structure before and after first column yielding occurred from HHT spectra. Table 3 and Fig. 8 indicate the results of RB vs. RES from FFT and HHT spectra in the TCG009 cases. The incremental increases between RB and RES can be seen clearly using HHT method after the RES<90%. Additionally, the change of RB at 1F can be found more obviously than those at the 3F in the initial yielding stage (RES=98.03%~76.11%) from HHT spectra. Next, the change of RB at 3F provides more sensitive than 1F when the PGA>0.6g. For example, the RB=1.2110 at 3F but the RB=1.1871 at 1F in the PGA=1.0g case. But the same phenomena cannot be seen from FFT results. The maximum RB is 1.0287 at 1F when PGA=0.4g but the RB reduces to 1.0072 while the PGA value reaches to 1.0g. Thus, there is no trend can be found in these cases from FFT spectra.

Fig. 9 shows the moment-rotation curve of the bottom of the first floor column in ten-story model for a predominant frequency of subjected to the adjusted PGA 921 (ILA061) earthquake. The hysteresis of these curves can be observed begging from PGA=0.28g case as shown in Table 3 and Fig. 9. Then the RES decreases with the increasing PGA values, for instance, the RES reduces to 36% while the PGA=1.0g. Figs. 10-12 display some results of acceleration response curves in the ten-story model using the FFT and HHT methods respectively. Fig. 10 shows the 1F and 10F FFT spectra (PGA=0.1g, 0.6g, 0.8g and 1.0g). The bandwidth of these four smoothed curves almost seems similarly whether the nonlinear behavior of structure occurred or not. Thus, the sensitivity of damage detection in ten-story model using FFT method is not good enough. Opposite to the FFT results, the change of bandwidth from HHT spectra can be observed clearly in the same cases as shown in Fig. 11. The bandwidth increases with an increasing PGA values after the member yielding occurred (PGA>0.28g).

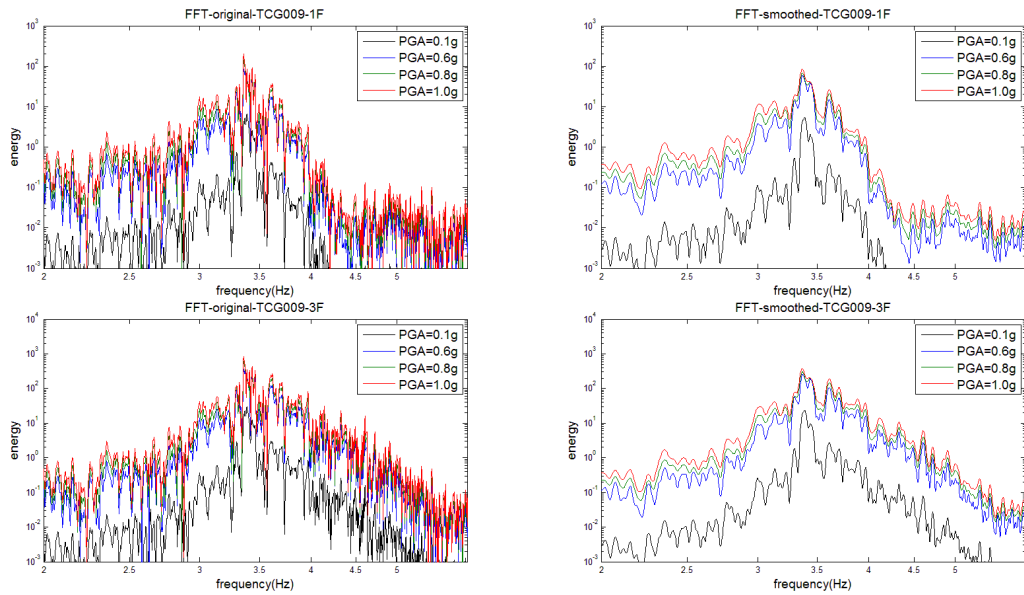


Fig. 6 Acceleration response spectra obtained using FFT for three -story cases (TCG009)

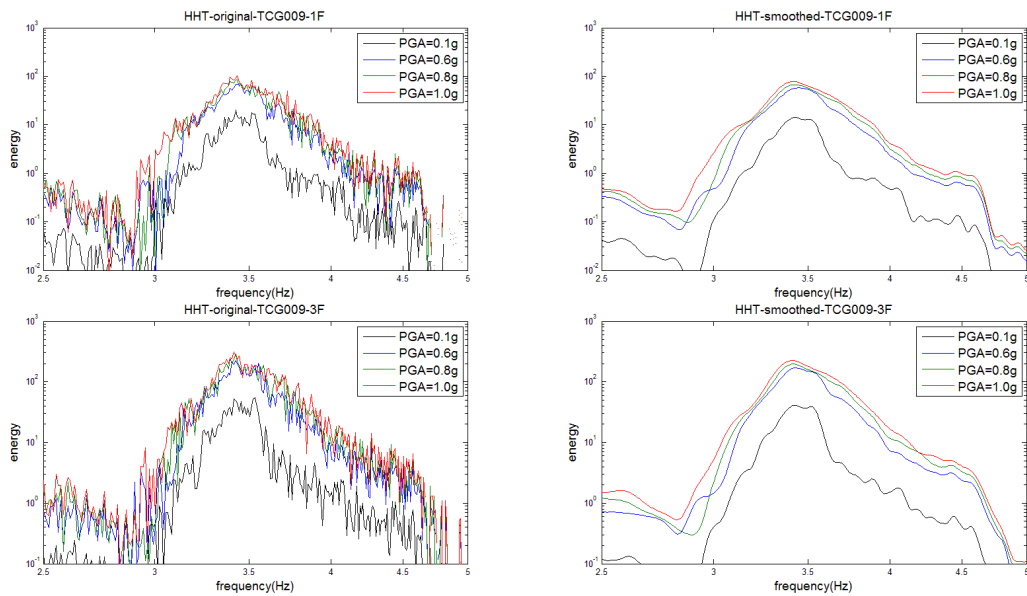


Fig. 7 Acceleration response spectra obtained using HHT for three -story cases (TCG009)

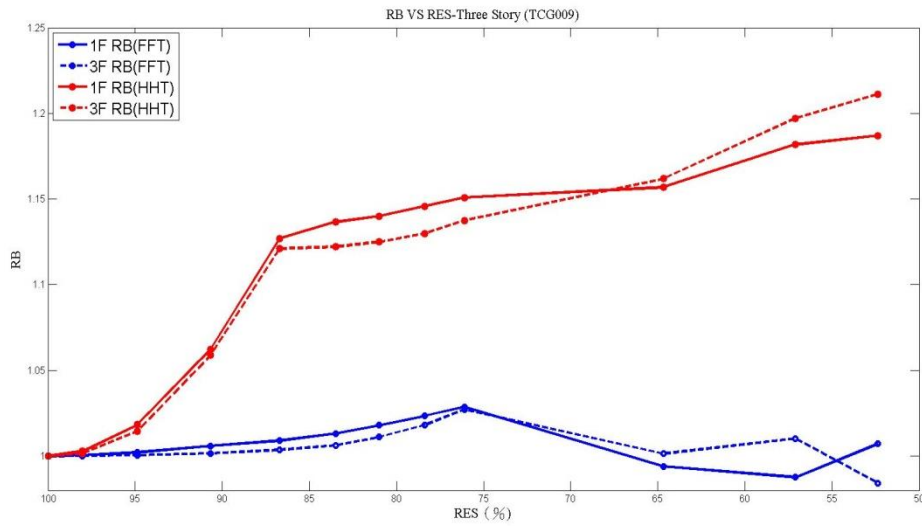


Fig. 8 Results of RB vs RES for three-story using FFT and HHT in the TCG009 cases

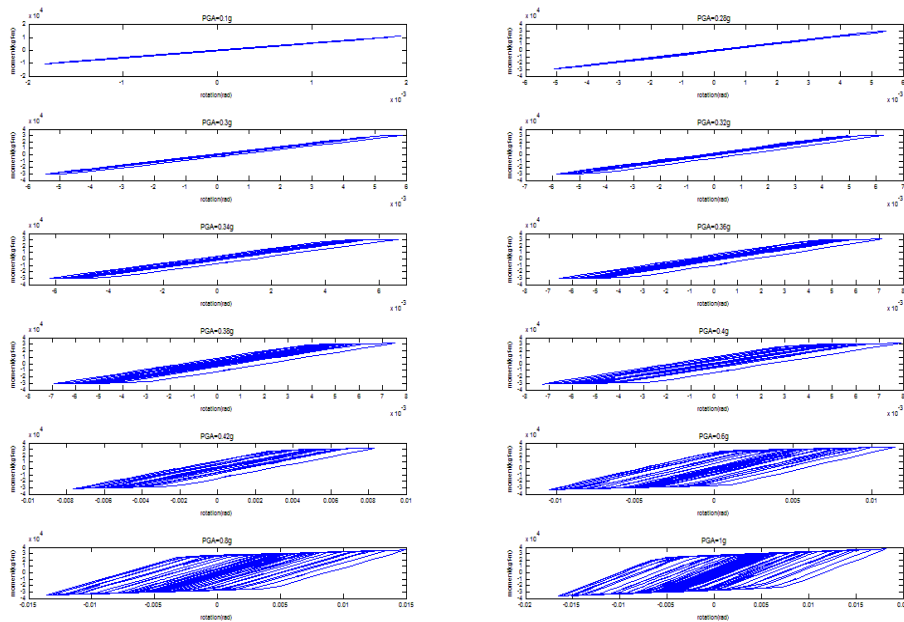


Fig. 9 Hysteresis of the bottom of the first floor column for ten-story cases (ILA061)

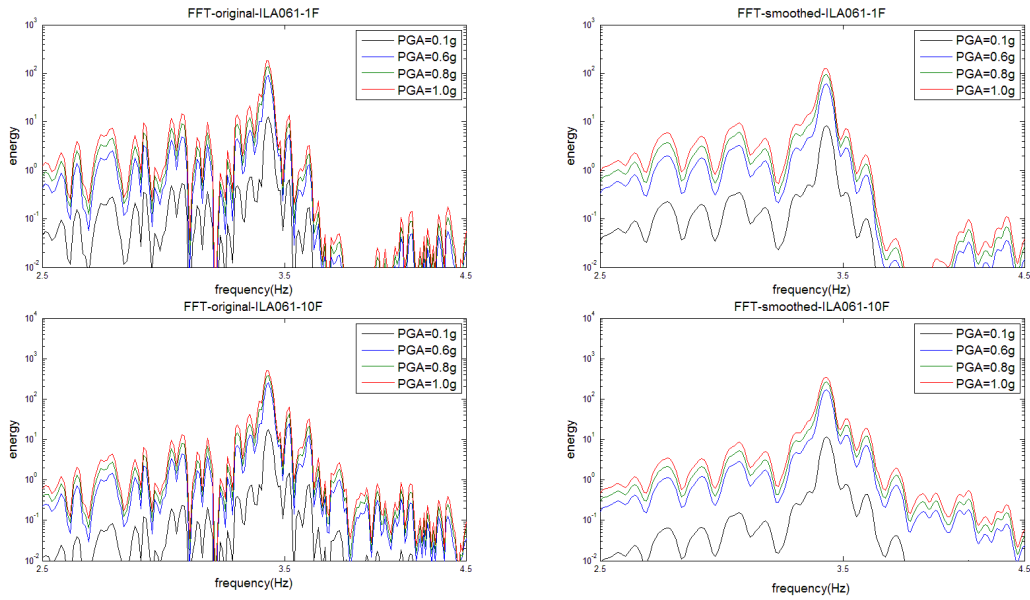


Fig. 10 Acceleration response spectra obtained using FFT for ten-story cases (ILA061)

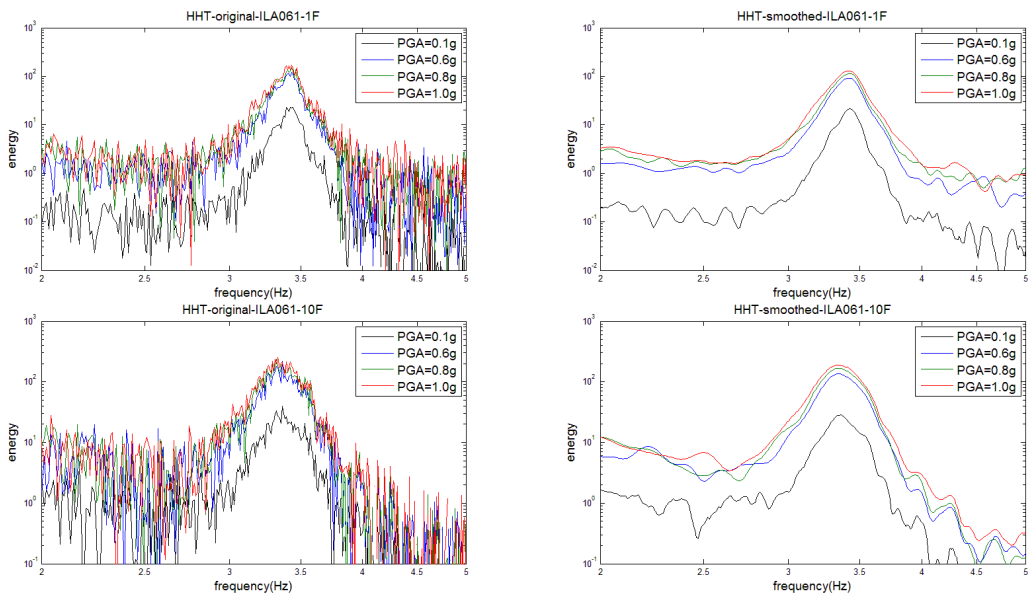


Fig. 11 Acceleration response spectra obtained using HHT for ten-story cases (ILA061)

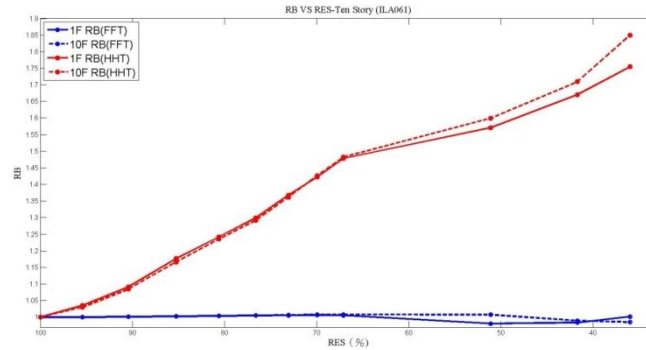


Fig. 12 Results of RB vs. RES for ten-story using FFT and HHT in the ILA061 cases

Fig. 12 indicates the analysis results of RB vs. RES for ten-story model based on FFT and HHT spectra in the 921 (ILA061) case. The RB almost keeps on 1.0 with the decreasing of RES. Even the heavy damage of the structure (RES=36%) happens, the change of RB still difficult to evaluate both at the 1F and 10F cases from FFT spectra as shown in Table 3 and Fig. 12. However the incremental trend of RB with RES can be found obviously from HHT results. Moreover the change of RB indicates more sensitive at 1F than that at 10F during the initial yielding stage (RES=100%~73.07%) presented from Fig. 12 and Table 3. But the change of RB still provides higher sensitive at 10F than 1F when the RES decreases heavily (RES<60%) in the ten-story ILA061 cases.

Fig. 13-18 display the results of RB with RES for three type structures in all cases from FFT and HHT spectra. In which, the change of RB with RES are summarized in Figs. 13, 15 and 17 based on FFT spectra. For example, the maximum value of RB is 1.0703 when the RES=93.78% in the TCU138 (3F) case as shown in Fig.13. Then the RB decreases with a decreasing RES, when the RES=56.54%, the RB reduces to 1.0535. Next, for ILA061 (1F) case, the RB almost retain around 1.0 when the RES=100%~72%. The change of RB can be observed when the RES<61.74% as shown in Fig.13. That is to say, in the FFT spectra, RB occasionally increases with decreasing RES, and occasionally decreases with RES. The same phenomena also can be seen in Figs. 15 and 17. For instance, the RB keeps around 1.0 in the five-story IWT026 (1F) case when the RES form 100% reduces to 38.33% as shown in Fig. 15. Moreover, only besides in the MYG010 and TCU138 cases, the RB almost has no change with RES in ten-story cases as shown in Fig. 17. Therefore, no steady trend of change is found for the RB vs. RES when analyzed with the FFT method.

Figs. 14, 16 and 18 indicate the analyzed results from HHT spectra. The positive trend of RB vs. RES can be found clearly for three-story model in all cases as shown in Fig. 14(a). For example, the change of RB can be observed (RB=1.0229 at 1F; RB=1.0203 at 3F) when the first column yielding occurred (RES=98.27%) in ILA061 case. Moreover the change of RB at 1F shows more sensitive than that at 3F in the initial yielding stage of three-story model as shown in Fig. 14(b). Next the RB increases with a decreasing RES both at 1F and 3F. When the RES<84.68%, the RB of 3F begins to larger than the RB at 1F. And the maximum of RB is 1.3683 at 3F when the RES reduces to 56.37% as shown in Fig. 14(a). It means that the change of RB at 1F shows higher sensitivity while the yielding of column just occurred. As the degree of damage goes on, the change of RB at 3F presents the highest sensitivity in detecting structural damage.

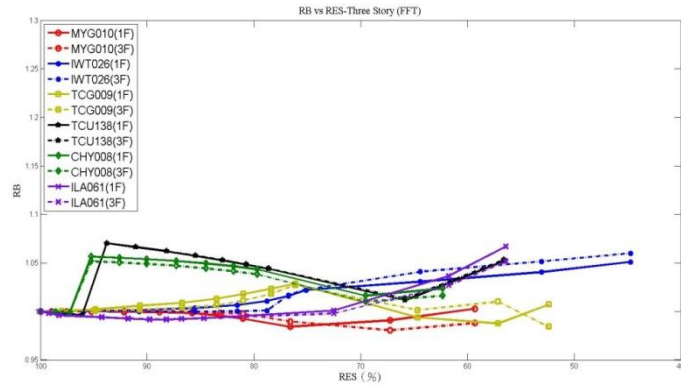
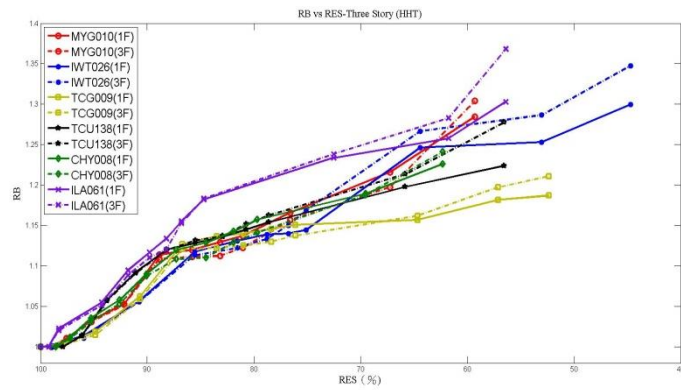
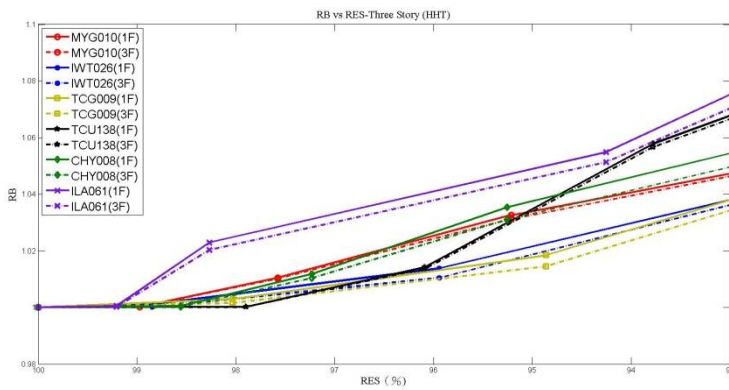


Fig. 13 Results of RB vs. RES using FFT for all cases (three-story)



(a)



(b)

Fig. 14 Results of (a) overall (b) zoom-in RB vs. RES using HHT for all cases (three-story)

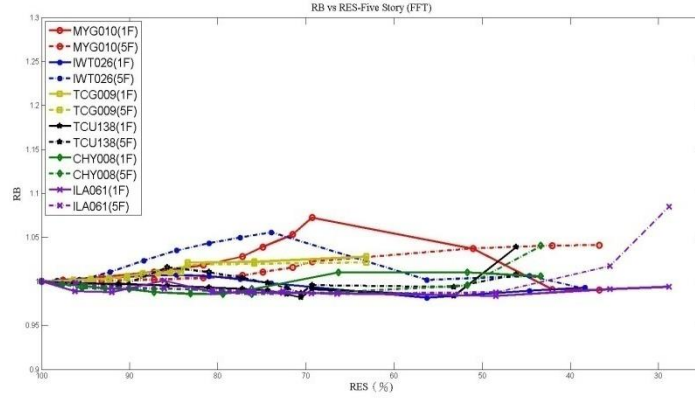
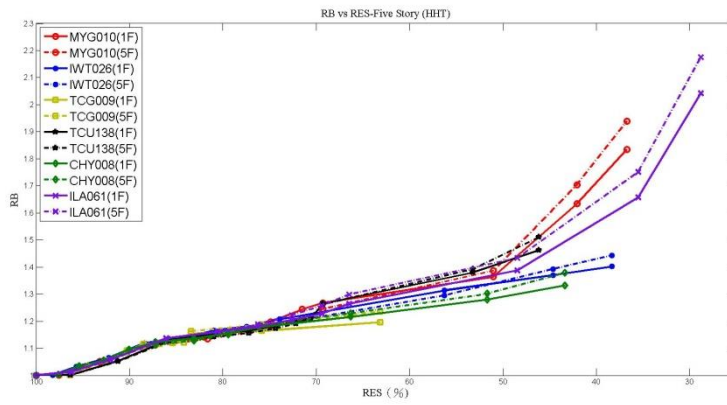
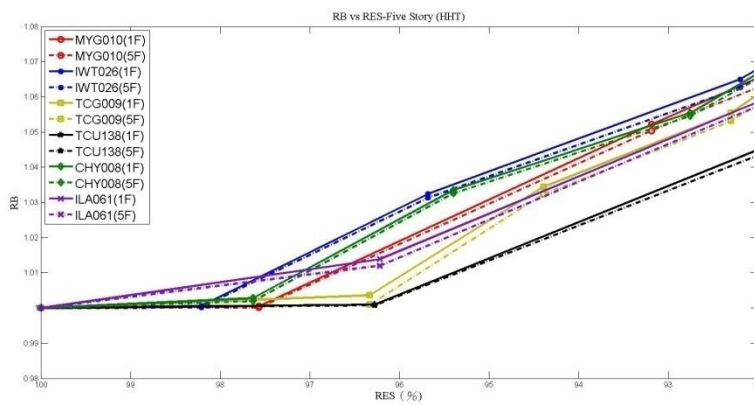


Fig. 15 Results of RB vs. RES using FFT for all cases (five-story)



(a)



(b)

Fig. 16 Results of (a) overall (b) zoom-in RB vs. RES using HHT for all cases (five-story)

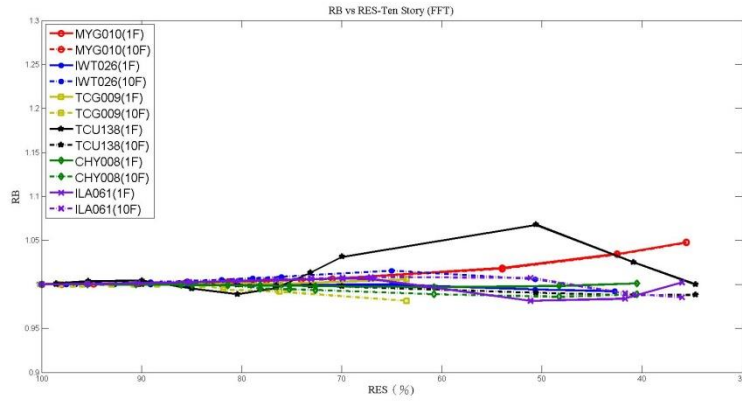
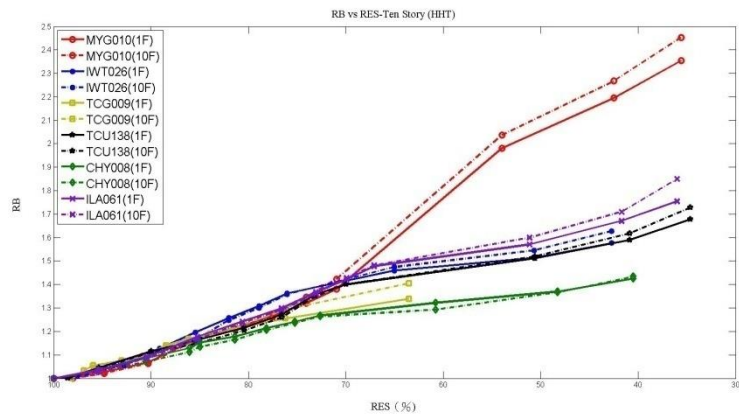
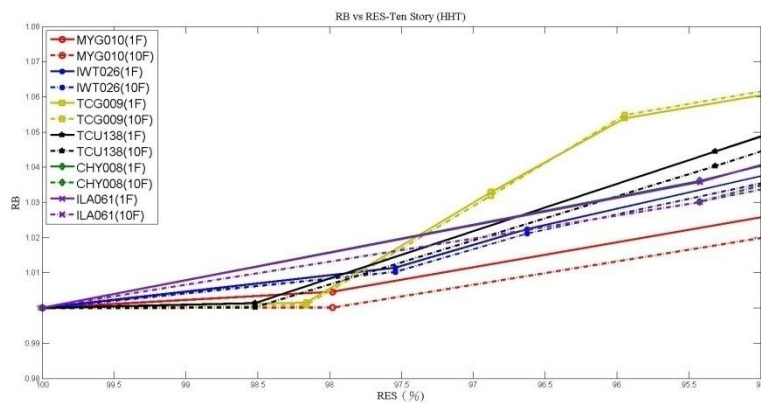


Fig. 17 Results of RB vs. RES using FFT for all cases (ten-story)



(a)



(b)

Fig. 18 Results of (a) overall (b) zoom-in RB vs. RES using HHT for all cases (ten-story)

Fig. 16 indicates RB vs. RES for five-story model in all cases using HHT method. After the first column yielding occurred ( $RES < 100\%$ ), RB displays the trend of incremental change with a decreasing RES from these curves as shown in Fig. 16(a). For instance, the maximum value of RB reaches to 2.1751 in ILA061 (5F) case when the RES reduces to 28.81%. From the results of the same case, the change of RB at 1F shows more sensitive than that at 5F in initial yielding stage of the five-story model as shown in Fig. 16(b). The similar analyzed results also can be obtained from ten-story cases as shown in Fig. 18. When the 1F column begins to yield ( $RES < 100\%$ ), the change of RB at 1F is larger than those at 10F as shown in Fig. 18(b). With the damage increasing, the incremental of RB at 10F is greater than RB at 1F as shown in Fig. 18(a). For instance, when the  $RES = 94.81\%$ , the  $RB = 1.0271$  at 1F but the  $RB = 1.0211$  at 10F in MYG010 case. Then the RES decreases with increasing structural damage, when the RES reduces to 35.59%, the RB increases to 2.3542 at 1F and the RB reaches to 2.4732 at 10F. Therefore, the change of RB at first yielding floor presents more sensitive than top floor. But when the damage grows up, the RB at top floor still shows the highest sensitivity for damage detection of a structure.

#### **4. Conclusions**

This study proposes the RB and RES as the damage detection indices to detect the structural damage of the steel structure to strong ground motions. Three type four bays MDOF steel models are constructed to subject the adjusted PGA Japan 311 and Chi-Chi 921 earthquakes. The acceleration response spectra evaluated from the first yielding floor and roof are using HHT and FFT methods respectively.

The simulation results indicate that the change of RB can be seen clearly when the  $RES < 90\%$  in all cases from HHT spectra. Moreover, the RB at first yielding floor changes more sensitive than those at roof when the response of a structure is in initial yielding stage ( $RES < 100\%$ ) from HHT spectra. With the nonlinear hysteresis grows up, the RB increases with a decreasing RES can be observed clearly especially the incremental change in RB at roof shows the highest sensitivity to detect the structural damage. Opposite to the results of HHT, the sensitive damage detection phenomena cannot be obtained from FFT spectra. The change of RB can be observed while the reduction of RES is large enough. However, there is no steady relationship between RB and RES from FFT spectra. Therefore, the damage detection index RB evaluated from HHT spectra presents more sensitive than FFT spectra. Moreover, the first yielding floor can be detected precisely and the structural damage can be observed in the top floor using damage detection index, RB from the HHT spectra.

#### **Acknowledgements**

The authors would like to thank Dr. Norden E. Huang, Director of the Adaptive Data Analysis Research Center at the National Central University, for his invaluable introduction to the HHT method and encouragement and advice for this study. The authors would like to thank the National Science Council of the Republic of China, Taiwan, for their financial support of this research under contract no. NSC 101-2221-E-008-077.

## References

- Alvanitopoulos, P.F., Andreadis, I. and Elenas, A. (2010), "Interdependence between damage indices and ground motion parameters based on Hilbert–Huang transform", *Meas. Sci. Technol.*, **21**(2), 025101-025114.
- Bindhu, K.R., Jaya, K.P. and Manicka Selvam, V.K. (2008), "Seismic resistance of exterior beam-column joints with non-conventional confinement reinforcement detailing", *Struct. Eng. Mech.*, **30**(6), 733-761.
- Chiang, W.L., Chiou, D.J., Chen, C.W., Tang, J.P., Hsu, W.K. and Liu, T.Y. (2011), "Detecting the sensitivity of structural damage based on the Hilbert-Huang transform approach", *Eng. Comput.*, **27**(7), 799-818.
- Chiou, D.J., Hsu, W.K., Chen, C.W., Hsieh, C.M., Tang, J.P. and Chiang, W.L. (2011), "Applications of Hilbert-Huang transform to structural damage detection", *Struct. Eng. Mech.*, **39**(1), 1-20.
- Chopra Anil, K. (2001), *Earthquake dynamics of structures: theory and applications to earthquake engineering*, 2nd Ed., 83.
- Chou, Y. (1975), *Statistical analysis*, 2nd Ed., New York: Holt Rinehart and Winston.
- Frank Pai, P. and Palazotto A.N. (2008), "HHT-based nonlinear signal processing method for parametric and nonparametric identification of dynamical systems", *Mech. Sci.*, **50**(12), 1619-1635.
- Gokdag, H. and Kopmaz, O. (2009), "A new damage detection approach for beam-type structures based on the combination of continuous and discrete wavelet transforms", *J. Sound Vib.*, **324**(3-5), 1158-1180.
- Han, J.P., Qian, J. and Zheng, P.J. (2011), "Structural damage identification based on Hilbert-Huang Transform and verification via shaking table model test", *Adv. Mater. Res.*, **255-260**, 4237-4241.
- Hsu, W.K., Huang, P.C., Chang, C.C., Chen, C.W., Hung, D.M. and Chiang, W.L. (2011), "An integrated flood risk assessment model for property insurance industry in Taiwan", *Nat. Hazards*, **58**(3), 1295-1309.
- Hsu, W.K., Tseng, C.P., Chiang, W.L. and Chen, C.W. (2012), "Risk and uncertainty analysis in the planning stages of a risk decision-making process", *Nat. Hazards*, **61**(3), 1355-1365.
- Huang, N.E., Shen, Z., Long, S.R., Wu, M.C., Shih, H.H., Zheng, Q., Yen, N.C., Tung, C.C. and Liu, H.H. (1998), "The empirical mode decomposition and the Hilbert spectrum for nonlinear and non-stationary time series analysis", *Proc. R. Soc. 115 London A, The Royal Society*, 903-995.
- Huang, N.E., Shen, Z. and Long, S.R. (1999), "A new view of nonlinear water waves: The Hilbert spectrum", *Annu. Rev. Fluid Mech.*, **31**, 417-457.
- Kao, S.C. and Govindaraju, R.S. (2010), "A copula-based joint deficit index for droughts", *J. Hydrol.*, **380**(1-2), 121-134.
- Kim, H. and Melhem, H. (2004), "Damage detection of structures by wavelet analysis", *Eng. Struct.*, **26**(3), 347-362.
- Kunwar, A., Jha, R., Whelan, M. and Janoyan, K. (2013), "Damage detection in an experimental bridge model using Hilbert–Huang transform of transient vibrations", *Struct. Control Health Monit.*, **20**(1), 1-15.
- Kuok, S.C. and Yuen, K.V. (2012), "Structural health monitoring of Canton tower using Bayesian framework", *Smart Struct. Syst.*, **10**(4-5), 375-391.
- Lanata, F. and Del Grosso, A. (2006), "Damage detection and localization for continuous static monitoring of structures using a proper orthogonal decomposition of signals", *Inst. Phys. Publishing Smart Mater. Struct.*, **15**, 1811-1829.
- Lei, Y., Kiremidjian, A.S., Nair, K.K., Lynch, J.P., Law, K.H., Kenny, T.W., Carryer, E.D. and Kottapalli, A. (2003), "Statistical damage detection using time series analysis on a structural health monitoring benchmark problem", *Proceedings of the 9th International Conference on Applications of Statistics and Probability in Civil Engineering*, San Francisco, CA, USA, July, 6-9.
- Lin S., Yang, J.N. and Zhou, L. (2005), "Damage identification of a benchmark building for structural health monitoring", *Smart Mater. Struct.*, **14**(3), 162-169.
- Maung, T., Than, M., Soe, T.T. and Tint, L.S. (2009), "Earthquake and Tsunami Hazard in Myanmar", *J. Earthq. Tsunami*, **3**(2), 43-57.
- Nair, K.K. and Kiremidjian, A.S. (2009), "Derivation of a damage sensitive feature using the haar wavelet transform", *Appl. Mech.*, **76**(6), 1-9.

- Raufi, F. (2010), "Damage detection in moment frame building by using Hilbert-Huang transform", *Proceedings of the Signal Processing Systems (ICSPS), 2nd International Conference*, July, **3**, 634-637.
- Ren, W.X. and Sun, Z.S. (2008), "Structural damage identification by using wavelet entropy", *Eng. Struct.*, **30**(10), 2840-2849.
- Pines, D. and Salvino, L. (2006), "Structural health monitoring using empirical mode decomposition and the Hilbert phase", *J. Sound Vib.*, **294**(1-2), 97-124.
- Rucka, M. and Wilde, K. (2006), "Application of continuous wavelet transform in vibration based damage detection method for beams and plates", *J. Sound Vib.*, **297**, 536-550.
- Sharma, A. Reddy, G.R., Eligehausen, R., Vaze, K.K., Ghosh, A.K. and Kushwaha, H.S. (2010), "Experiments on reinforced concrete beam-column joints under cyclic loads and evaluating their response by nonlinear static pushover analysis", *Struct. Eng. Mech.*, **35**(1), 99-117.
- Shiau, J.T., Wang, H.Y. and Tsai, C.T. (2006), "Bivariate frequency analysis of floods using copulas", *J. AM. Water Resour.*, **42**(6), 1549-1564.
- Sohn, H., Farrar, C.R., Hemez, F.M., Shunk, D.D., Stinemates, D.W. and Nadler, B.R. (2003), *A review of structural health monitoring literature: 1996–2001*, Los Alamos National Laboratory Report, LA-13976-MS.
- Su, S.C., Huang, N.E. and Wen, K.L. (2008), "A new spectral representation of strong motion earthquake data: Hilbert spectral analysis of Tai-power building station, 1994~2006", *Proceedings of the 5th Int. Conf. on Urban Earthquake Engineering*, Tokyo, Japan.
- Sun, Z. and Chang, C.C. (2002), "Structural damage assessment based on wavelet packet transform", *J. Struct. Eng. -ASCE*, **128**(10), 1354-1361.
- Tang, J.P., Chiou, D.J., Chen, C.W., Chiang, W.L., Hsu, W.K., Chen, C.Y. and Liu, T.Y. (2011), "A case study of damage detection in benchmark buildings using a Hilbert-Huang Transform-based method", *J. Vib. Control*, **17**(4), 623-636
- Wang, J.F., Lin, C.C. and Yen, S.M. (2007), "A story damage index of seismically-excited buildings based on modal frequency and mode shape", *Eng. Struct.*, **29**(9), 2143-2157.
- Wen, Y.K. (1976), "Method for random vibration of hysteretic system", *J. Eng. Mech. – ASCE*, **102**(2), 249-263.
- Wu, Z. and Huang, N.E. (2004), *Ensemble empirical mode decomposition: a noise-assisted data analysis method*, Centre for Ocean-Land-Atmosphere Studies, Tech. Rep, **173**.
- Yang, J.N. and Lei, Y. (2000a), "System identification of linear structures using Hilbert transform and empirical mode decomposition", *Proceedings of the 18th Int. Modal Analysis Conf.: A Conf. on Structural Dynamics, Society for Experimental Mech., Inc., Bethel, Conn.*, **1**, 213-219.
- Yang, J.N. and Lei, Y. (2000b), "Identification of civil structures with nonproportional damping", *Proc. SPIE*, **3988**, 284-294.
- Yang, J.N., Lei, Y., Pan, S. and Huang, N. (2003a), "Identification of linear structures based on Hilbert-Huang transform. Part I: Normal modes", *Earthq. Eng. Struct. D.*, **32** (9), 1443-1467.
- Yang, J.N., Lei, Y., Pan, S. and Huang, N. (2003b), "Identification of linear structures based on Hilbert-Huang transform. Part II: Complex modes", *Earthq. Eng. Struct. D.*, **32** (10), 1533-1554.
- Yang, J.N, Lei, Y., Lin, S. and Huang, N. (2004), "Hilbert–Huang based approach for structural damage detection", *J. Eng. Mech - ASCE*, **130**(1), 85-95.
- Yu, L. and Giurgiutiu, V. (2005), "Advanced signal processing for enhanced damage detection with piezoelectric wafer active sensors", *Smart Struct. Syst.*, **1**(2), 185-215.
- Zhanga, X., Wong, K.K F. and Wang, Y. (2007), "Performance assessment of moment resisting frames during earthquakes based on the force analogy method", *Eng. Struct.*, **29**(10), 2792-2802.
- Zhang, P.R., Ma S., Safak, E. and Hartzell S. (2003), "Hilbert-Huang transform analysis of dynamic and earthquake motion recordings", *J. Eng. Mech.- ASCE*, **129**(8), 861-875.
- Zhang, J. and Xu, S.Y. (2009), "Seismic response simulations of bridges considering shear-flexural interaction of columns", *Struct. Eng. Mech.*, **31**(5), 545-566.